Mansoura Engineering Journal

Volume 48 | Issue 1 Article 14

2023

Zero-Sequence Current in Cable Systems: A Study

Shimaa A. F. Salem
MSc Student, North Delta Electric Distribution Company (NDEDC), Mansoura, Egypt, shimaa.ammar89@gmail.com

Rabab R. M. Eiada
Assistant Professor New Damietta High Institute of Engineering and Technology, Ministry of High Education, New Damietta, Egypt, rabab.reda@ndeti.edu.eg

Ebrahim A. Badran
Professor Electrical Engineering Department, Faculty of Engineering, Mansoura University, Mansoura , Egypt

ORIGINAL STUDY

Zero-sequence Current in Cable Systems: A Study

Shimaa A.F. Salem [a,*], Rabab R.M. Eiada [b], Ebrahim A. Badran [c]

[a] North Delta Electric Distribution Company (NDEDC), Mansoura, Egypt
[b] New Damietta High Institute of Engineering and Technology, Ministry of High Education, New Damietta, Egypt
[c] Electrical Engineering Department, Faculty of Engineering, Mansoura University, Mansoura, Egypt

Abstract

Large zero-sequence current is not a new phenomenon for cable bus duct systems; the question is what influences its magnitude. It was found that the zero-sequence currents were circulating between different circuits in the cable system and that they were being generated by induction between phases in the same cable route. It was determined that the zero-sequence currents could be greatly reduced in a twin circuit by a symmetrical configuration of the cables. However, in a four-circuit system, no significant reduction could be achieved even by the symmetrical configuration. Therefore, in this paper, this phenomenon will be analyzed and discussed. ATPDraw is used to simulate and analysis this kind of study. Also, the effect of sheath cross-bonding is explained and analyzed. It is found that the currents are changed dramatically according to the arrangement of each cable. When reducing zero-sequence currents, various layouts are examined in light of their underlying physical causes. Also, It is determined that the zero-sequence current is hardly affected by any unbalanced crossbondig

Keywords: Cables arrangement, Current distribution, Sheath cross bonding, Zero-sequence currents

1. Introduction

With the power consumption in cities increasing continuously, the capacities of single-core cables need to be extended. At present, two schemes were widely used: one was to directly replace the previous cables with larger-capacity cables; another was to added cables in the same phase to put into operation in parallel. As the replacement scheme needed longer outage time and greater investment, the parallel scheme was always seen as the optimum scheme in practice. However, after been applied, the current distribution in parallel single-core cables was not even as expected. This phenomenon may cause the overheating problem in parts of the cables. It had been estimated that an increase of 8 °C−10 °C in insulation temperature was lead to a 50% reduction of insulation life expectancy (Petty, 1988; Li et al., 2015).

High-power DC rectifier/converter design is a key focus of electrochemical applications. Due to the high current magnitudes involved, additional cable geometry considerations are made to achieve the necessary current balance in parallel rectifier cells (Bernadelli et al., 1997). The majority of industrial rectifiers employ l2-pulse converters, which phase shift one converter with regard to the other by 30° (Tambe and Frisch, 2004).

Despite the high-current secondary windings not being grounded, depending on the input cable geometry and the converter's operational characteristics, a zero-sequence ground current (I_{ZS}) may flow (Skibinski et al., 2006). In industrial and commercial power distribution networks, underground cables are increasingly used for power transmission. In many cases, one substation will send out two or more transmission lines, and one line may include double circuits. Therefore, in some cases, cables from two or more circuits are put in ducts side by side along the same route for several kilometres. When numerous circuits are built on one tower, it is also known that each circuit of overhead transmission cables is saturated with I_{ZS}. The zero-

Received 24 August 2022; revised 12 November 2022; accepted 20 November 2022.
Available online 12 June 2023

* Corresponding author. Tel.: +201557657070.
E-mail address: shimaa.ammar89@gmail.com (S.A.F. Salem).

https://doi.org/10.58491/2735-4202.3039

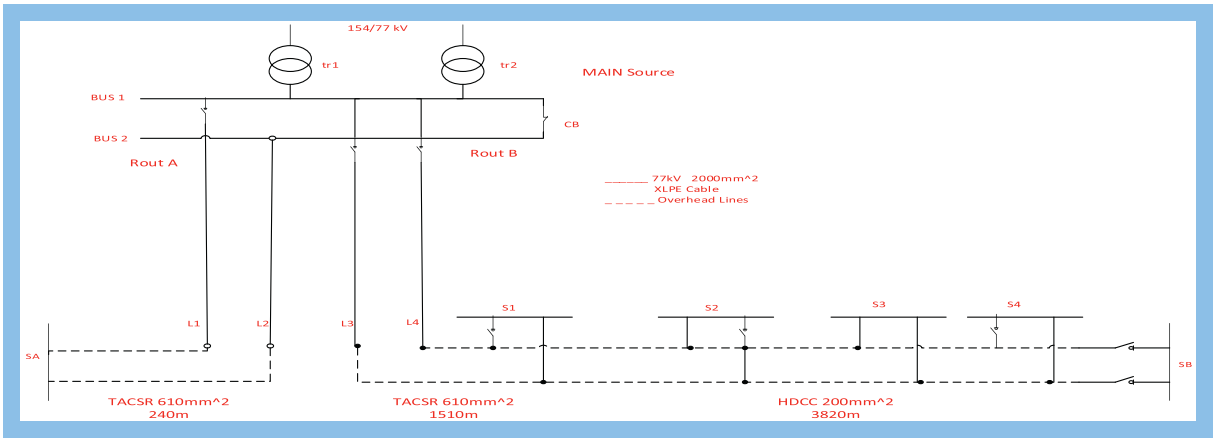

Fig. 1. Test system single line diagram.

sequence currents are an issue because they can occasionally make safety relays malfunction. However, it has not been well understood that systems with many cables deployed along the same path generate I_{ZS}. Depending on the cable configuration, such as that of an untransposed overhead line, the impedance imbalance between the phases cannot be ignored (Nakanishi et al., 1991).

On a single-core cable, the impacts of earthing, cross-bonding, and transposition procedures are investigated, along with the number of joint sites. It was found that the produced voltages and currents were related to cable length and that, in addition to neutralizing the cable ends, cross-bonding and transposition processes were the only ways to lower them (Gouramanis et al., 2011; Kaloudas et al., 2011; Shokry et al., 2019; Ledari and Mirzaie, 2020; Salem et al., 2022).

In this paper, a cable system was recently found, where a very large amount of I_{ZS} flows. For this study in a test power system, the Alternative Transients Program (ATP) analyses the I_{ZS}. Typical two- and four-circuit cable systems are examined to show that large I_{ZS} are induced in the cable systems. It is shown that the currents are changed dramatically according to the arrangement of each cable. In light of their physical sources, several arrangements are tested to lower I_{ZS}. Also highlighted are certain issues with zero-sequence circulating current cabling. Therefore, the paper organization is give as follows. An introduction to the problem is given in section 1. The test system description and simulation is explained in section 2, and in section 3 the system is analyzed in fault and abnormal operating conditions. Then, induced zero-sequence currents are simulated and modeled in section 4. In section 5, the effect of sheath cross-bonding is discussed. Finally, the conclusions and future work are given in section 6.

2. Test system description and simulation

The test system is picked from reference (Nakanishi et al., 1991). Fig. 1 illustrates the configuration of the test system. The main substation S is linked to a 154 kV line. Transformers lower the voltage to 77 kV, and the power is distributed to substations SA, SB, and S1 to S4 via cables and overhead lines. Transformers at each substation further lower the incoming 77 kV–6.6 kV, which is subsequently supplied to customers via distribution lines.

2.1. Transformers description

A computation that takes into account the impact of the earth return current and transformer inductance includes the transformer in the main substation. The transformer is connected star–star, and its neutral point is grounded by connecting a 200 Ω resistor in parallel to a series circuit made up of 260 mH inductors and a 15 Ω resistor. For distribution in the substations at the load side, the voltage is reduced to 6.6 kV. Although a resistor grounds the main substation transformer's neutral point when using a star–delta connection, the neutrals of the transformers S1–S4 are not earthed (Nakanishi et al., 1991).

Table 1. Parameters of 77 kV, 2000 mm^2 XLPE Cable.

Type of cable	Single core, 2000 mm^2 XLPE
Outer core diameter	53.8 mm
Inner sheath diameter	90.2 mm
Overall diameter	99.2 mm
Resistivity of core	1.7E-8 Ω m
Resistivity of sheath	2.5E-8 Ω m

Table 2. Arrangements of 77 kV, 2000 mm² XLPE Cable.

Rout	Cable	Section 1 (64 m)		Section 2 (44.8 m)		Section 3 (74.7 m)		Section 4 (35 m)		Section 5, 6, 7 and 8 (175.2 m, 290.3 m, 335.8 m And 309.2 m)		Section 9 (79.3 m)	
		V	H	V	H	V	H	V	H	V	H	V	H
	A1	1.9	0	2.7	0	5.23	0	2.9	0	2.4	0	2.7	0
Route A (L1)	B1	1.9	0.3	2.45	0	5	−1.3	2.65	0	2.4	−0.225	2.45	0
	C1	1.9	0.6	2.2	0	5.23	−1.3	2.4	0	2.175	0	2.45	−0.25
	A2	2.2	0.6	2.2	−0.25	5.23	−1.53	2.4	−0.25	1.95	−0.45	2.45	−0.5
Route A (L2)	B2	2.2	0.3	2.45	−0.25	5	−1.53	2.65	−0.25	2.175	−0.45	2.7	−0.5
	C2	2.2	0	2.7	−0.25	5.23	−0.23	2.9	−0.25	2.175	−0.225	2.7	−0.25
	a1	1.6	0.6	3.2	0	5	0	3.15	0	2.85	0	3.2	0
Route B (L3)	b1	1.6	0.3	2.95	0	5.23	−0.46	3.15	−0.25	2.85	−0.225	2.95	0
	c1	1.6	0	2.95	−0.25	5	−0.23	3.4	0	2.625	0	2.95	−0.25
	a2	1.3	0	2.95	−0.5	5.23	−0.69	3.15	−0.5	2.4	−0.45	2.95	−0.5
Route B (L4)	b2	1.3	0.3	3.2	−0.5	5	−0.69	3.4	−0.5	2.625	−0.45	3.2	−0.5
	c2	1.3	0.6	3.2	−0.25	5	−0.46	3.4	−0.25	2.625	−0.225	2.7	0

H, Horizontal position; Where V, Vertical position.

2.2. Cables description

Table 1 shows the parameters of the 77 kV, 2000 mm² XLPE Cable. Sheath-circuits are grounded through 10 Ω resistors at two terminal ends. The cable configuration of four Routes A and B circuits is shown in Table 2. Every section of routes A and B has two cables, and each section of a PI equivalent circuit with 24 conductors simulates the changing cable configurations and sheath terminating conditions.

2.3. Overhead lines description

Table 3 shows the lines parameters (Cable, 2009; 'Indian Standard for Hard, 1982). A PI equivalent circuit's single section is used to represent the lines. The placement of the overhead lines along routes A and B is depicted in Table 4.

2.4. Load description

During the calculation, star connection load resistance is simulated. Not earthed is the load neutral. The measured load flow via each circuit of examples (a) to (d) led to the calculation of the load resistance linked to each circuit, which is given in Table 5 (Nakanishi et al., 1991).

Table 3. Parameters of 610 mm² TACSR and 200 mm² HDCC Overhead lines.

Type of conductor	TACSR 610 mm²	HDCC 200 mm²
Component of stranded wires	Al 54/3.80, AC 7/3.80	19/3.65 mm
Total inner diameter	11.4 mm	0
Total diameter	34.2 mm	18.2 mm
DC resistance at 20 °C	0.0458 Ω/km	0.09020 Ω/km

Table 4. Arrangements of 610 TACSR and 200 mm² HDCC Overhead lines.

Rout	Line	V	H
Route A (L1)	A1	33.4	2.5
	B1	36.3	2.5
	C1	30.5	2.5
Route A (L2)	A2	33.4	−2.5
	B2	36.3	−2.5
	C2	30.5	−2.5
Route B (L3)	a1	25.8	2.75
	b1	28.6	2.6
	c1	23	2.9
Route B (L4)	a2	25.8	−2.75
	b2	28.6	−2.6
	c2	23	−2.9

2.5. Test system simulation by ATPDraw

ATP is used to analyze the current distribution in the system with several scenarios of the fault and abnormal operating conditions (Rifaldi and Lastra, 2001). The test system is simulated using ATPDraw as shown in Fig. 2.

An AC (type 14) three-phase, the voltage source is selected for source simulation. The Hybrid three-

Table 5. Measured results of load flow (current, A).

CASES	Route A		Route B	
	L1	L2	L3	L4
Case (a)	260	330	0	0
Case (b)	250	350	400	0
Case (c)	250	340	0	480
Case (d)	250	350	230	200

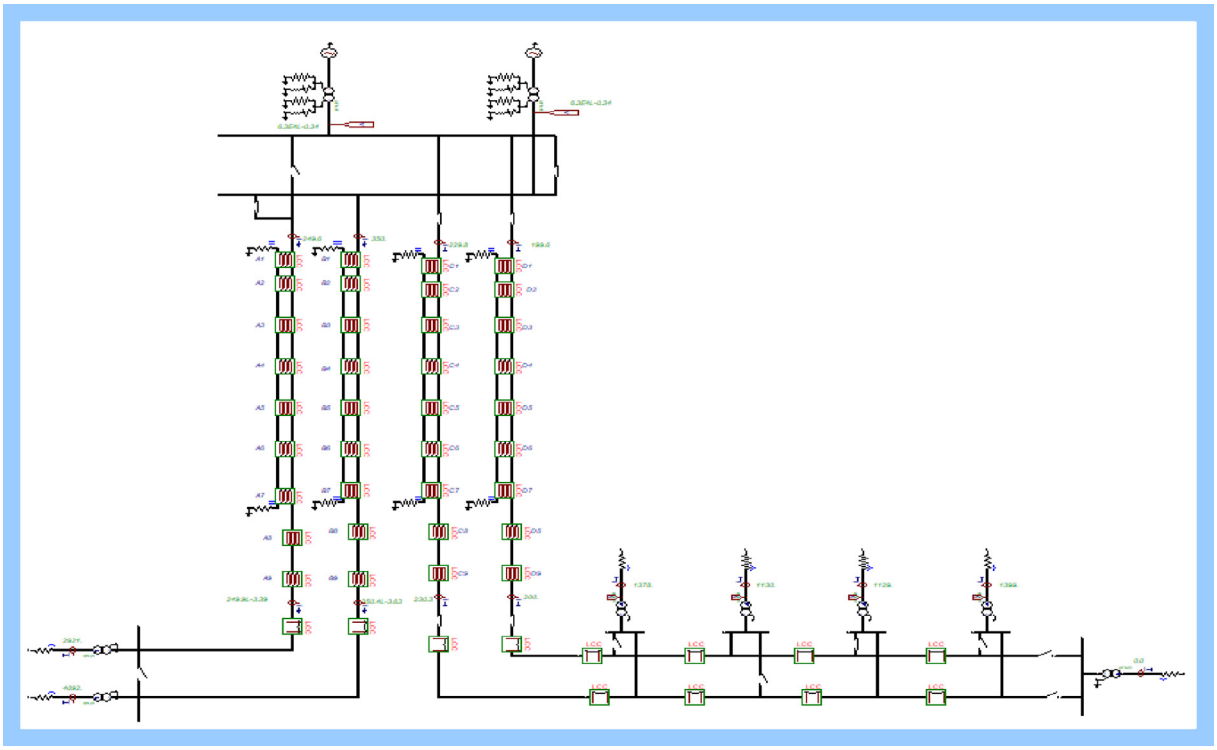

Fig. 2. Test system simulation using ATPDraw.

phase transformer model is used for transformer simulation. Also, the three-phase time-controlled switch is used for switch simulation.

The three-phase single-core cables are modeled using LCC (line cable constant) model as shown in Fig. 3. The number of phases is 6 to simulate sheath circuits, (1, 2, 3) number of cable phases and (4, 5, 6) number of sheath circuits. Also, the three-phase overhead lines are modeled using LCC model of PI equivalent circuit.

A PI equivalent circuit's single section with 24 conductors is used to simulate each section of the route A and B cables when the cable arrangement and sheath terminating condition change. A PI equivalent circuit's single section is used to simulate the overhead lines as well. The load RLC-Y, three-phase is used for load simulation.

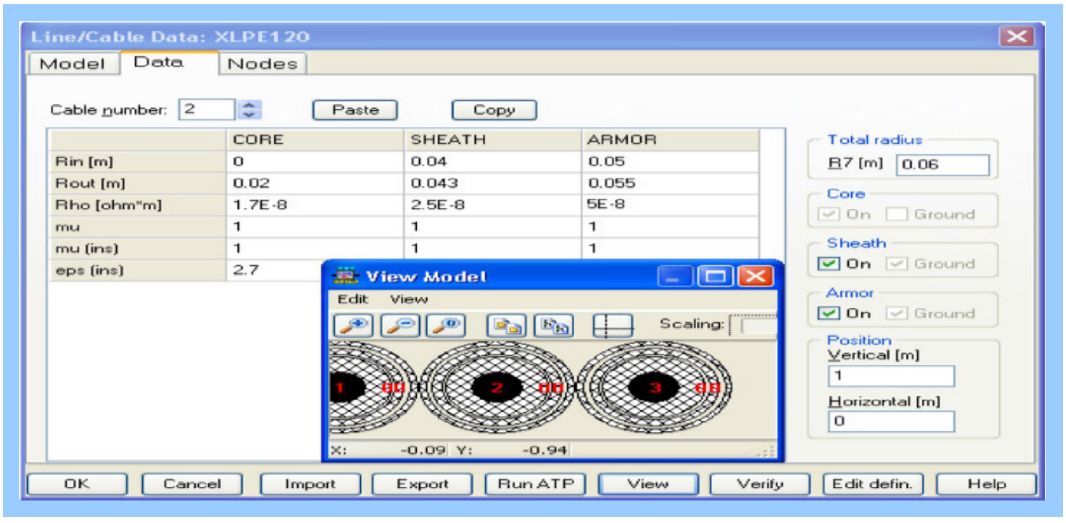

Fig. 3. Cable data dialog box for a three-phase single core type.

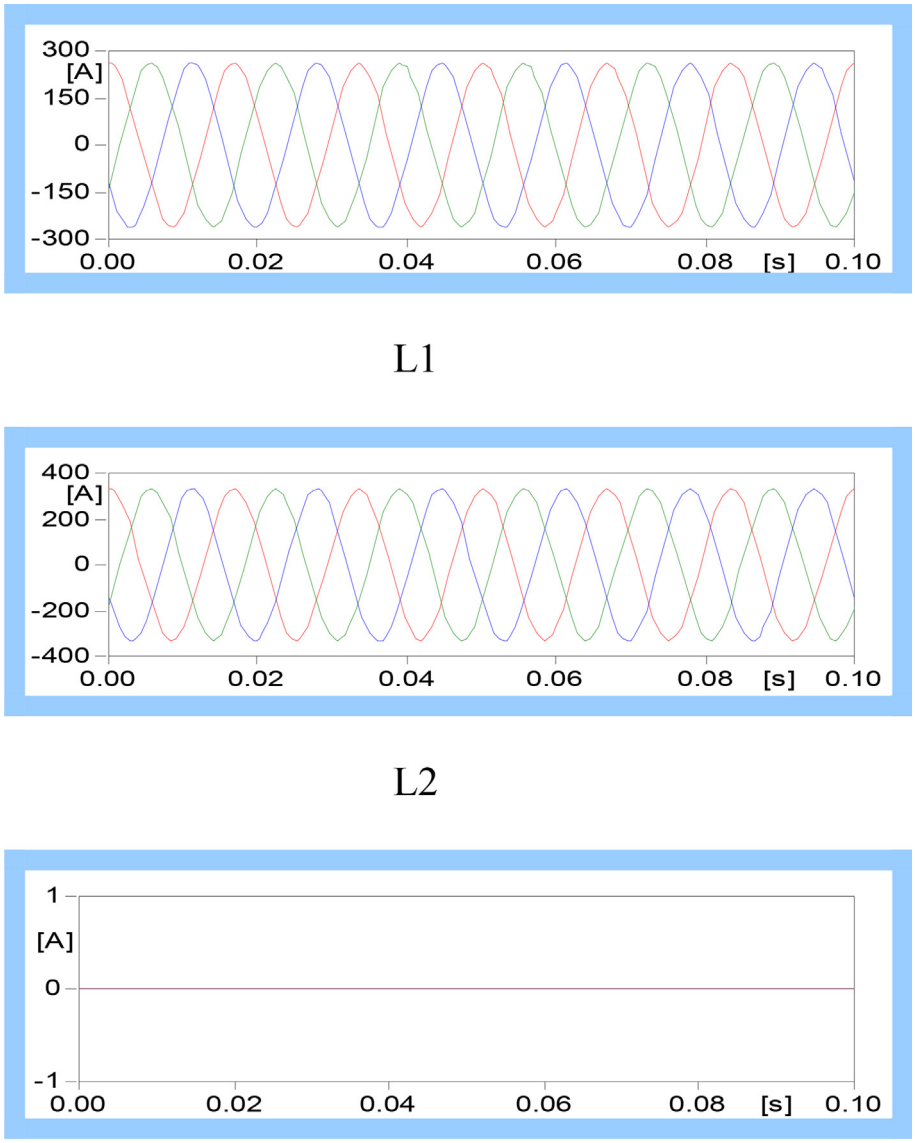

Fig. 4. The calculated currents for Case (a).

3. Analysis of the test system for fault and abnormal operating conditions

Power flow through each circuit is calculated via the following scenarios of the system; case (a) to (d).

In case (a), there are two circuits connected. Bus 2 is connected with route A. While route B are separated from the bus and the cable separated from the line. Fig. 4a and b illustrate the output current waveform in route A. It is shown that the current is about 260 A through cable (L1) and about 330 A through cable (L2). Fig. 4c illustrates the output current waveform in route B. It is shown that the current is 0 A through cables (L3&L4).

In case (b) three circuits are connected. Route A is connected to Bus 2. While (L3) is connected to Bus 1 and (L4) is separated from the bus. Also, the cable separated from the line, and the remote end is separated from SB. Fig. 5a and b illustrate the output current waveform in route A. It is shown that the current is 250 A through cable (L1) and 350 A through cable (L2). Fig. 5c and d illustrate the output current waveform in route B. It is shown that the current is 400 A through cable (L3) and 0 A through cable (L4).

In case (c) three circuits are connected. Route A is connected to Bus 2. While (L3) is separated from the

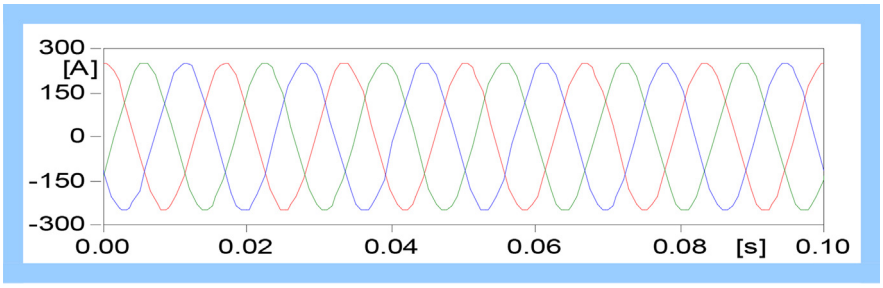

(a) L1

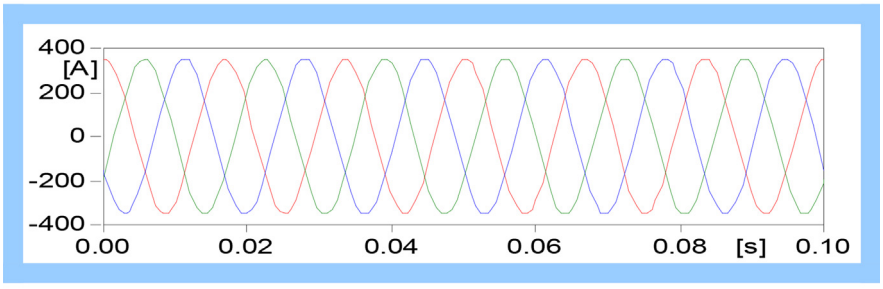

(b) L2

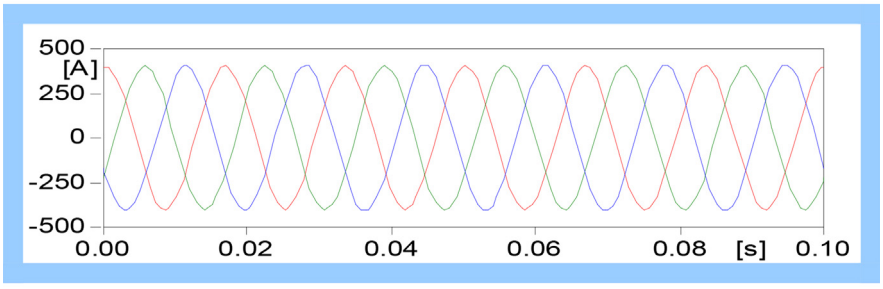

(c) L3

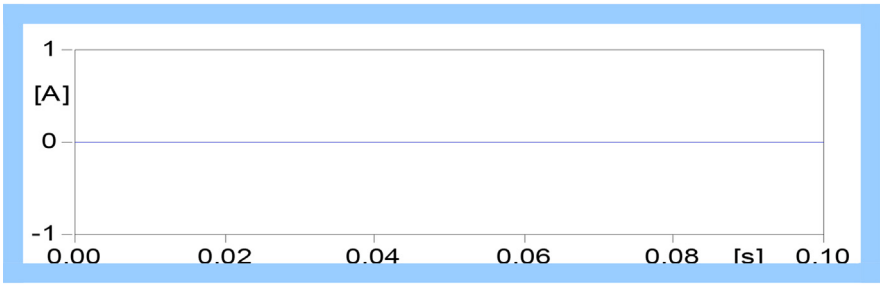

(d) L4

Fig. 5. The calculated currents for Case (b).

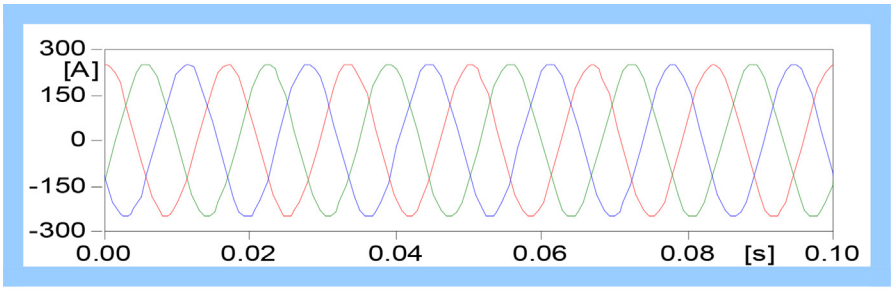

(a) L1

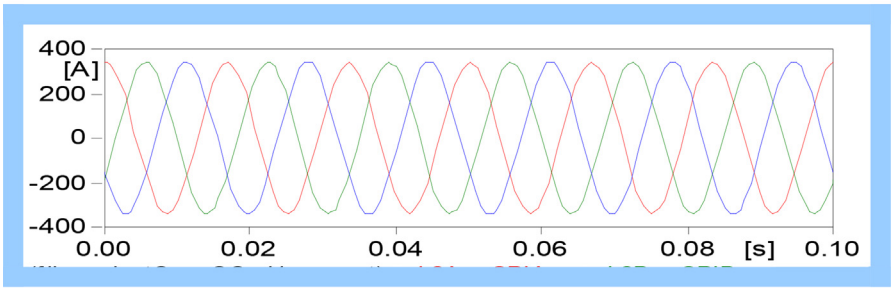

(b) L2

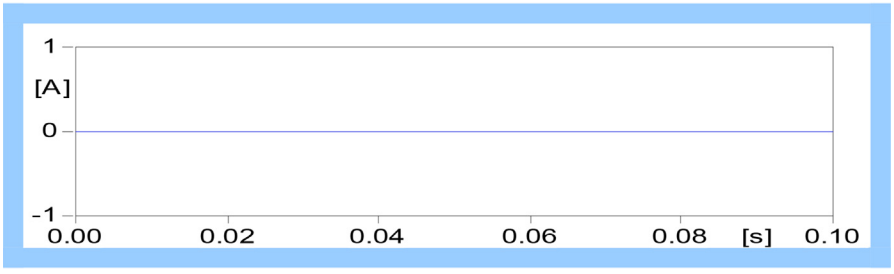

(c) L3

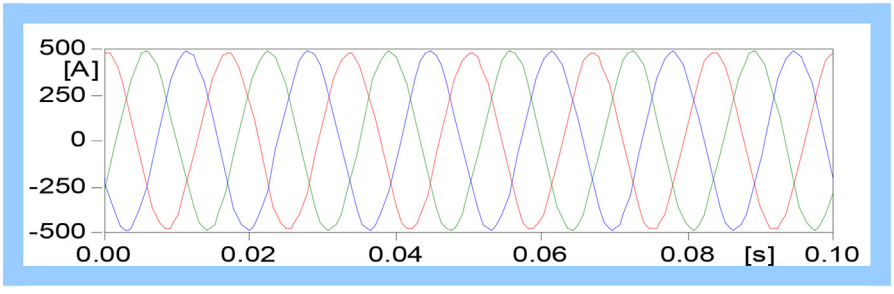

(d) L4

Fig. 6. The calculated currents for Case (c).

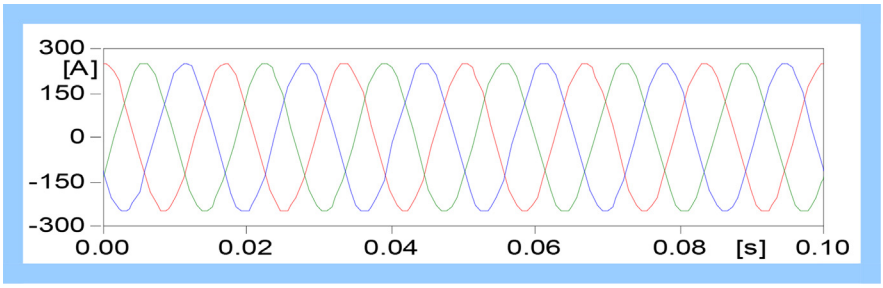

(a) L1

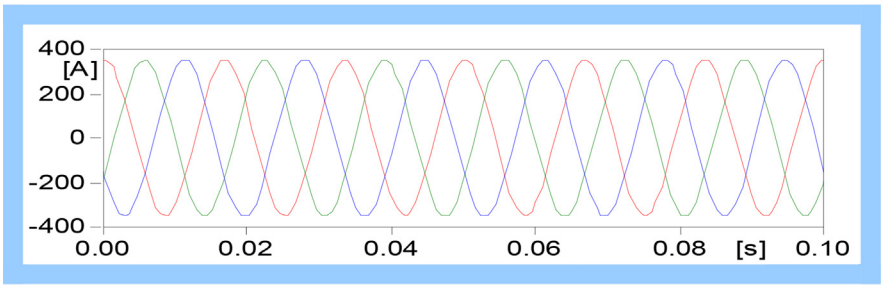

(b) L2

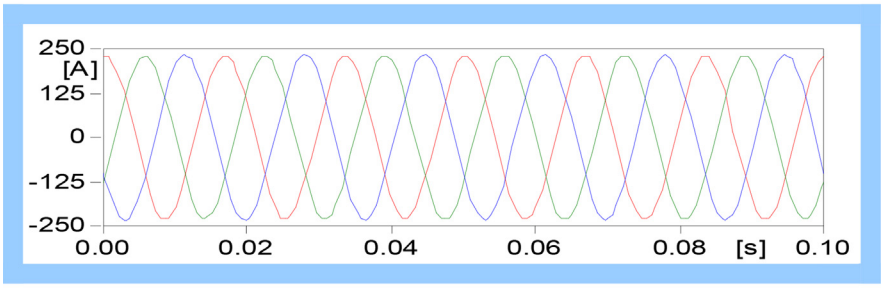

(c) L3

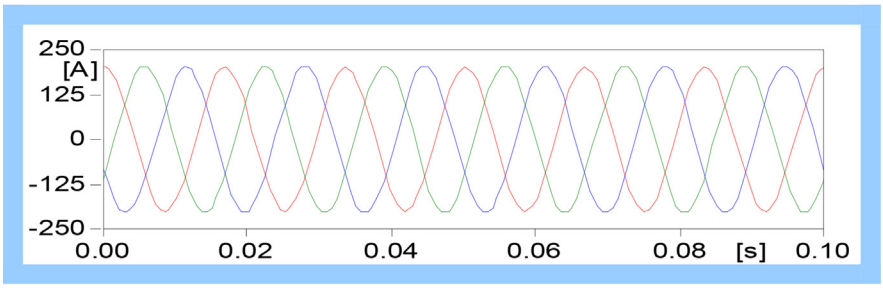

(d) L4

Fig. 7. The calculated current for case (d).

Table 6. Measured results of Izs for rout A and B (current, A).

Cases	Route A		Route B	
	L1	L2	L3	L4
Case (a)	38	38	0	0
Case (b)	60	66	0.1	0
Case (c)	78	78	0	0.5
Case (d)	66	66	15	15

bus also, the cable separated from the line, and (L4) is connected to Bus 1. Farther end of the overhead line separated from SB. Fig. 6a and b illustrate the output current waveform in route A. It is shown that the current is 250 A through cable (L1), and 350 A through cable (L2). Fig. 6c and d illustrate the output current waveform in route B. It is shown that the current is 0 A through cable (L3) and 430 A through cable (L4).

Table 7. Parameters of 77 kV, 1000 mm^2 XLPE Cable.

Type of cable	Single core, 1000 mm^2 XLPE
Outer core diameter	38 mm
Inner sheath diameter	57.3 mm
Overall diameter	79 mm
Resistivity of core	1.7E-8 Ω m
Resistivity of sheath	2.5E-8 Ω m

In case (d) four circuits are connected. Bus 2 is linked to Route A (L1, L2). Bus 1 is also connected to route B (L3, L4), but SB is separated from the receiver end of the overhead transmission line. Fig. 7a and b illustrate the output current waveform in route A. It is shown that the current is 250 A through cable (L1), and 350 A through cable (L2). Fig. 7c and d illustrate the output current waveform in route B. It is shown that the current is 230 A through cable (L3) and 200 A through cable (L4).

It is found that the results confirm the model validity by comparing with (Nakanishi et al., 1991).

The above observations indicate that the ATP-Draw simulation provides great accuracy in comparison to the measured data, despite using PI equivalence for the simulation's cables to be represented. Therefore, it may be sufficient to analyze the I_{ZS} using the ATPDraw with PI equivalent model of the cables. Table 6 shows the measured results of I_{ZS} for cases (a) to (d). A large I_{ZS} of 40–80 A was observed on route A (Nakanishi et al., 1991).

The following conclusions are drawn about I_{ZS} based on the data in Table 6 Case (a) only has two

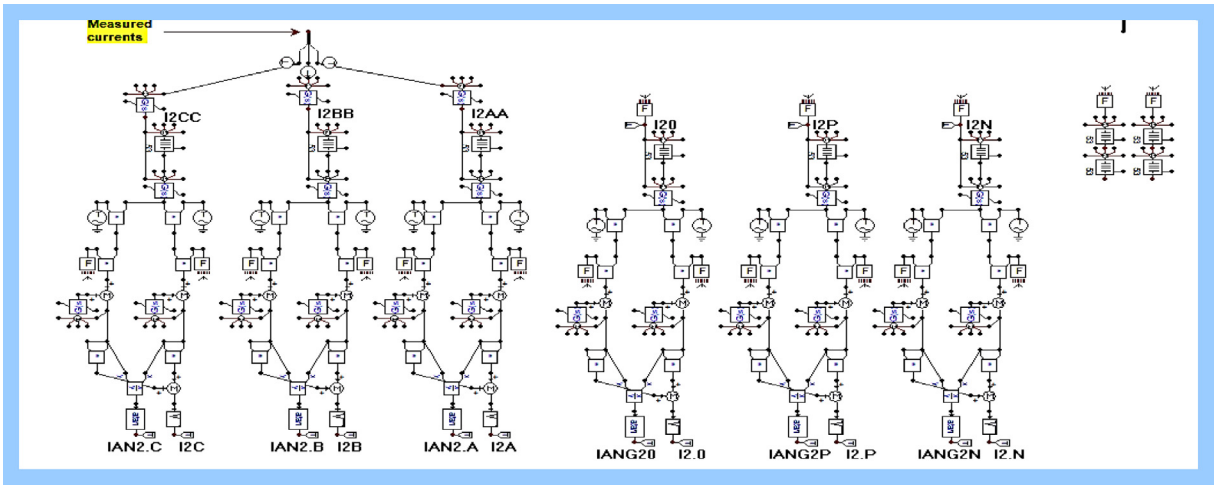

Fig. 8. ATPDraw model for currents calculations.

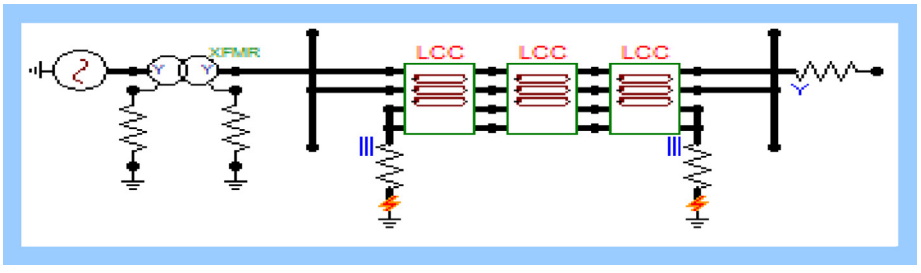

Fig. 9. The twin-circuit system model in ATPDraw.

Table 8. Various cable arrangements for a twin circuit (Take A1 reference).

cable	Case 1		Case 2		Case 3		Case 4		Case 5		Case 6	
	V	H	V	H	V	H	V	H	V	H	V	H
A1	1.6	0	1.6	0	1.6	0	1.6	0	1.83	0	1.6	0
B1	1.83	0	1.83	0	1.83	0	1.83	0	2.06	0	1.83	0
C1	2.06	0	2.06	0	2.06	0	2.06	0	2.06	0.23	1.83	0.23
A2	1.6	0.46	2.06	0.23	1.6	0.46	1.6	0.23	1.83	0.46	1.83	0.46
B2	1.83	0.46	1.83	0.23	1.83	0.46	1.83	0.23	1.6	0.46	1.6	0.46
C2	2.06	0.46	1.6	0.23	2.06	0.46	2.06	0.23	1.6	0.23	1.6	0.23

cable	Case 7		Case 8		Case 9		Case 10		Case 11	
	V	H	V	H	V	H	V		V	H
A1	1.83	0	1.6	0	1.6	0	1.6	0	1.6	0
B1	2.06	0	1.83	0	1.83	−0.23	1.6	0.23	1.6	0.23
C1	2.06	0.23	1.83	0.23	2.06	−0.23	1.6	0.46	1.6	0.46
A2	1.6	0.23	1.6	0.23	2.06	0.23	1.6	0.69	1.6	1.15
B2	1.6	0.46	1.6	0.46	1.83	0.23	1.6	0.92	1.6	0.92
C2	1.83	0.46	1.83	0.46	1.6	0.23	1.6	1.15	1.6	0.69

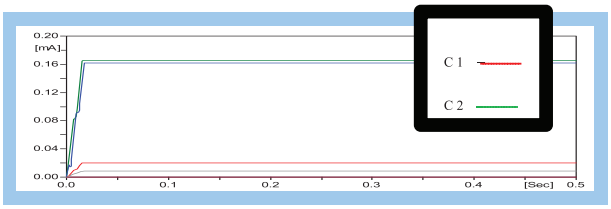

(a) Cable L1 for C 1 to C 6

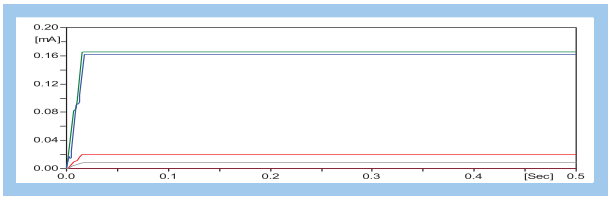

(b) Cable L2 for C 1 to C 6

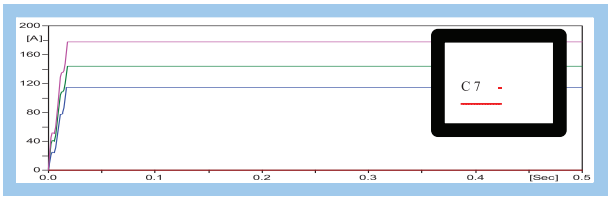

(c) Cable L1 for C 7 to C 11

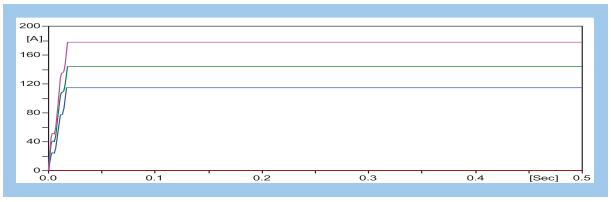

(d) Cable L2 for C 7 to C 11

Fig. 10. The calculated I_{ZS} in twine-circuit for all cases.

circuits, route A (L1, L2). Here, an I_{ZS} is generated between L1 and L2, with the currents having the same amplitude but an opposite direction. The loop circuit of the main source, S, L1, SA, L2, and then back to the main source, S, is shown to be circulating the I_{ZS}. Cases (b) and (c) are systems that have three circuits of route A (L1 and L2), and route B (L3 or L4). L3 and L4 of route B do not carry any I_{ZS}. The neutrals of the transformers S1 to S4 are not earthed, however, the neutral of the main S transformer is through a resistor. As a result, it is impossible to complete the loop circuit using the earth as the return path, and no I_{ZS} is produced in one circuit. A multi-circuit system's I_{ZS} is observed to be the vector sum of the I_{ZS} in both its own circuit and those induced by the other circuit (Nakanishi et al., 1991).

4. Analysis of the induced zero-sequence current

4.1. Calculation of I_{ZS} in ATPDraw

The information in this section is a summary of research on parallel-two and parallel-four circuits that create I_{ZS}. After that, this knowledge is expanded upon to explain the I_{ZS} in a parallel six

Table 9. Results of I_{ZS} in a twin-circuit system.

arrangement	I_{ZS} (A)	arrangement	I_{ZS} (A)
case(1)	2.0343E-5	case(7)	1.8486E-3
case(2)	8.2310E-6	case(8)	144.27
case(3)	4.6838E-8	case(9)	114.89
case(4)	5.8053E-8	case(10)	177.71
case(5)	1.6198E-4	case(11)	1.0256E-7
case(6)	1.6573E-4		

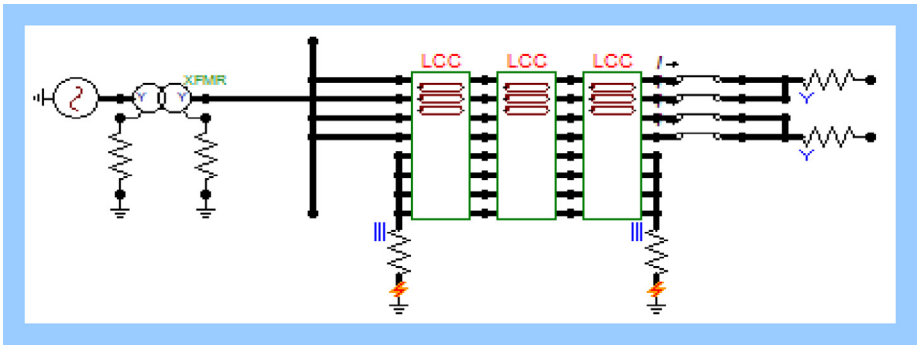

Fig. 11. System model in ATPDraw for four circuits.

cable bus duct circuit (twine circuit). According to the test system, the model system's voltage class is set at 77 kV. The model system consists of one main crossbonded cable section and three smaller parts, each measuring 250 m. A 77 kV/1000 mm^2 XLPE cable is used.

Table 7 shows this cable parameters (Nexans, 2009). While taking conductor and sheath into account, each minor section is represented by a PI equivalent circuit's single section. Both of the cable's sheaths are grounded by a 10 Ω resistor and are short circuited at both ends. The load is represented by 44.5 Ω, three-phase, and star-connections. The load is balanced, star-connection resistor. The neutral point of the load is not earthed.

An extraction of the fundamental I_{ZS} can be performed according to equations (1)–(3) (Badran and Abdel-rahman, 2010).

$$\begin{bmatrix} i_{ap} \\ i_{bp} \\ i_{cp} \end{bmatrix} = \frac{1}{3} \begin{bmatrix} i_a - \frac{1}{2}(i_b + i_c) + j\frac{\sqrt{3}}{2}(i_b - i_c) \\ -(i_{ap} + i_{cp}) \\ i_c - \frac{1}{2}(i_a + i_b) + j\frac{\sqrt{3}}{2}(i_a - i_b) \end{bmatrix} \quad (1)$$

Table 10. Various cable arrangements in a four-circuit (Take a1 reference).

cable	Case 1		Case 2		Case 3		Case 4		Case 5	
	V	H	V	H	V	H	V	H	V	H
a1	1.6	0	1.6	0	2.06	0	2.06	0	1.6	0
b1	1.83	0	1.83	0	2.29	0	2.29	0	1.83	0
c1	2.06	0	2.06	0	2.29	0.23	2.29	0.23	2.06	0
a2	1.6	0.23	2.06	0.23	2.29	0.46	2.29	0.46	1.6	0.23
b2	1.83	0.23	1.83	0.23	2.06	0.46	2.06	0.46	1.83	0.23
c2	2.06	0.23	1.6	0.23	2.06	0.23	2.06	0.23	2.06	0.23
a3	1.6	0.46	1.6	0.46	1.6	0	1.83	0	2.06	0.46
b3	1.83	0.46	1.83	0.46	1.83	0	1.83	0.23	1.83	0.46
c3	2.06	0.46	2.06	0.46	1.83	0.23	1.83	0.46	1.6	0.46
a4	1.6	0.69	2.06	0.69	1.83	0.46	1.6	0.46	2.06	0.69
b4	1.83	0.69	1.83	0.69	1.6	0.46	1.6	0.23	1.83	0.69
c4	2.06	0.69	1.6	0.69	1.6	0.23	1.6	0	1.6	0.69

$$\begin{bmatrix} i_{an} \\ i_{bn} \\ i_{cn} \end{bmatrix} = \frac{1}{3} \begin{bmatrix} i_a - \frac{1}{2}(i_b + i_c) + j\frac{\sqrt{3}}{2}(i_b - i_c) \\ -(i_{ap} + i_{cp}) \\ i_c - \frac{1}{2}(i_a + i_b) + j\frac{\sqrt{3}}{2}(i_a - i_b) \end{bmatrix} \quad (2)$$

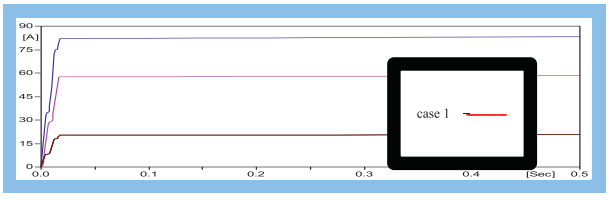

(a) Cable L1

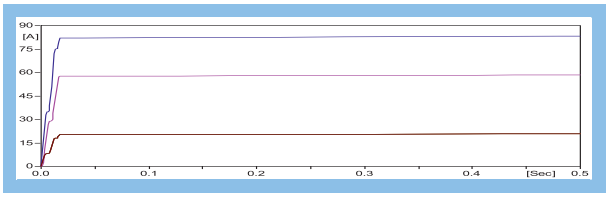

(b) Cable L2

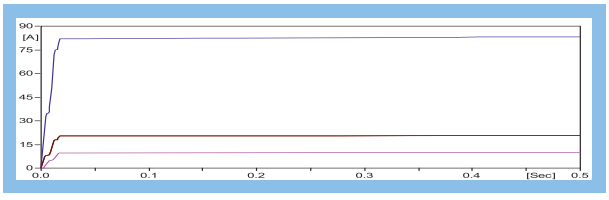

(c) Cable L3

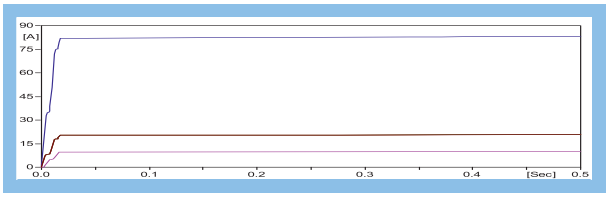

(d) Cable L4

Fig. 12. Calculated I_{ZS} currents in four-circuit for all cases.

Table 11. The results I_{ZS} in four circuits.

Cable	zero sequence current (A)			
	L1	L2	L3	L4
case(1)	20.537	20.537	20.537	20.537
case(2)	20.571	20.571	20.571	20.571
case(3)	82.638	82.638	82.638	82.638
case(4)	57.963	57.963	9.8262	9.8262
case(5)	20.571	20.571	20.571	20.571

$$\begin{bmatrix} i_{a0} \\ i_{b0} \\ i_{c0} \end{bmatrix} = \frac{1}{3} \begin{bmatrix} (i_a + i_b + i_c) \\ (i_a + i_b + i_c) \\ (i_a + i_b + i_c) \end{bmatrix} \quad (3)$$

Where i_a, i_b, and i_c are the measured phase currents for phase A, B, and C, respectively. Also, i_{ap}, i_{bp}, and i_{cp} are three-phase positive sequence components; i_{an}, i_{bn} and i_{cn} are three-phase negative sequence components, and i_{a0}, i_{b0}, and i_{c0} are three-phase zero-sequence components for the three-phases, respectively. The ATPDraw model of the current's calculations given in equations (1)–(3) is illustrated in Fig. 8.

4.2. Analysis of I_{ZS} in a twin-circuit

In a nine-duct configuration test system with twin parallel circuits, the change of cable arrangements is discussed (Nakanishi et al., 1991). The test system is model using ATPDraw as shown in Fig. 9. Zero-sequence current is the vector sum of the I_{ZS} in its own circuit and the currents generated by the other parallel circuits in zero-sequence. Different cable configurations in the model system of Fig. 9, twin circuits in parallel in a nine duct layout, are given as shown in Table 8 (case 1 to case 11) as follow:

(1) Low Reactance Phasing (LR Phasing) is a type of phasing arrangement where cases (1) and (2) are inversely arranged, and case 1 is an arrangement where there is no conduit between L1 and L2.
(2) Super-Bundle Phasing (SB Phasing) is used to describe Cases (3) and (4), and Case (3) is the arrangement where the conduit line between L1 and L2 is left empty of Cases (4).
(3) Case 5 and 6 are defined as triangular arrangement of L1 and L2 and point symmetrical to the center of 6 cables.
(4) In case (7), a diagonal-shaped empty conduit line is formed by the arrangement of L1 and L2, which are triangularly arranged and axially symmetrical to it.
(5) Cases (8) to (10) are the asymmetrical arrangements of the cables between circuits L1 and L2.
(6) In cases 10 and 11, an underground cable that is directly buried and axially symmetrical is assumed.

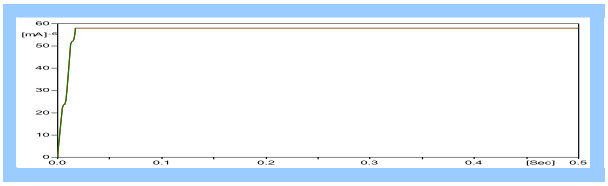

(a) conductor

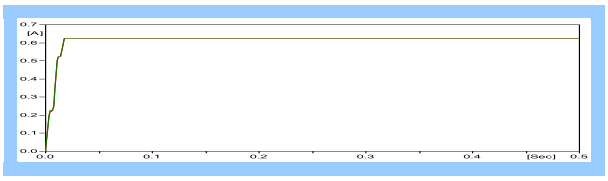

(b) sheath

Fig. 13. Calculated I_{ZS} for case (4) balanced cross bonding.

Fig. 10 shows the results of I_{ZS} flows at cable L1 and L2 in cases (1) to (11). Table 9 gives the I_{ZS} in all cases. It is noted from Table 9 that low I_{ZS} flows with symmetrical arrangements (1) to (7) and (11). However, for the asymmetrical arrangements (8) to (10), I_{ZS} of 144–178 A flow for the same load currents. Math analysis of the parallel two-circuit cases proves the required condition to insure no I_{ZS} is to have all mutual impedance's between conductors balanced (Nakanishi et al., 1991). Proper conductor phasing arrangements can accomplish this. A zero I_{ZS} condition corresponds to point or axial symmetry of the six-conductors in the two parallel circuits and indicates an asymmetrical arrangement of cable is the cause of I_{ZS} generation. That is to say, the mutual impedance unbalance generates the I_{ZS} in the twin circuit.

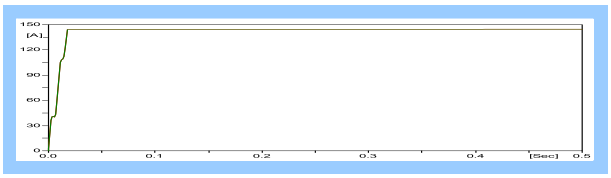

(a) Conductor

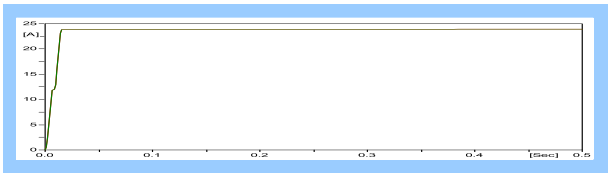

(b) Sheath

Fig. 14. Calculated I_{ZS} for case (8) balanced cross bonding.

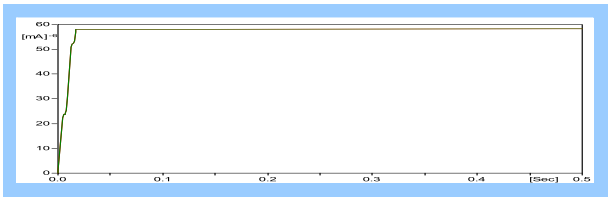

(a) conductor

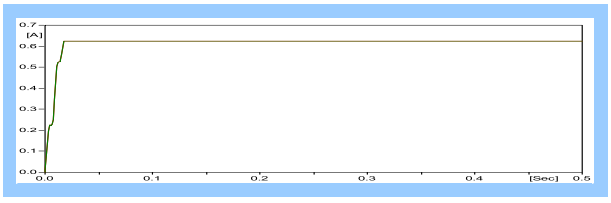

(b) sheath

Fig. 15. Calculated I_{ZS} for case (4) unbalanced cross bonding.

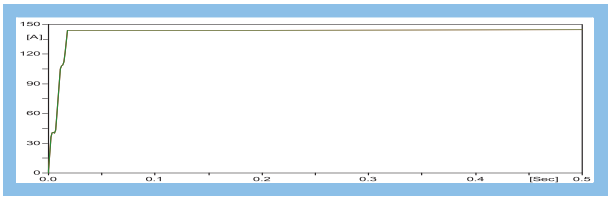

(a) conductor

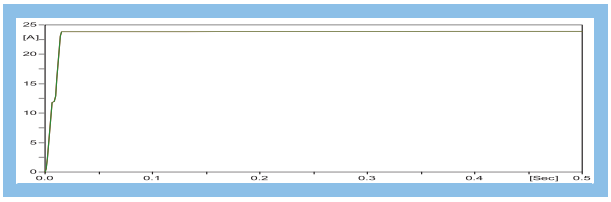

(b) sheath

Fig. 16. Calculated I_{ZS} for case (8) unbalanced cross bonding.

4.3. Analysis of I_{ZS} in a four-circuit system

The test system is represented using ATPDraw as illustrated in Fig. 11 in order to investigate I_{ZS} in a four-circuit system. In the system, a loop is formed by circuits L1 and L2 on route A and L3 and L4 on route B, respectively. Routes A and B are short-circuited at the opposite end for each phase.

Table 10 gives the various cable arrangements of twelve phases (case 1 to case 5) in a model system of Fig. 11; four circuits in parallel as follows:

(1) Super-Bundle Phasing (SB Phasing) arrangements are used in Cases (1) and (5), but route B is arranged in opposition to route A.
(2) Case (2) is used Low Reactance Phasing (LR Phasing) arrangements.
(3) Case (3) is a triangular configuration, while Case (4) combines a triangle (route A) and LR phasing (route B) configuration.
(4) In case (1), Routes A and B are axially symmetrical, while in cases (2), (3), and (5), they are point symmetrical.
(5) Case (4) is used asymmetrical arrangements.

Fig. 12 shows the results of I_{ZS} flows at cable L1 and L2 in cases (1) to (5). Table 11 gives the I_{ZS} in all cases. As can be seen from Table 11, unlike in the cases of two circuit systems, the I_{ZS} does not decrease to almost zero even with SB phasing or LR phasing design. At least 20 A of I_{ZS} must flow in addition to the conductor current of 500 A. With a triangular configuration, I_{ZS} can move at a maximum rate of 83 A. Zero-sequence currents vary with conductor phasing arrangement. The results show I_{ZS} generated due to unbalanced mutual coupling between the four parallel circuits. Four parallel circuits are unlike parallel two-circuit arrangements; I_{ZS} cannot be reduced to zero in parallel four-circuits, even with point or axial symmetry conductor configurations. The results show a minimum (I_{ZS}/ I_{load}) ratio of 4% can be expected. Conductor transposition is required to reduce I_{ZS} in a four-circuit cable duct system.

5. Effect of sheath cross bonding

The arrangements of Case (4), which has no I_{ZS} flowing, and Case (8), which has the maximum zero-sequence current flowing, are taken from Table 9 in order to analyse the effect of sheath cross bonding over I_{ZS} in twin-circuit systems. Additionally, calculations were done for two scenarios: balanced cross-bonding (each minor section was 250 m long) and unbalanced cross-bonding (length of minor section at 300 m-250 m–200 m). This section

Table 12. The results of Izs for sheath crosbonding

cases	cable	Arrangement (4)		Arrangement (8)	
		Conductor (A)	sheath (A)	conductor (A)	sheath (A)
balanced cross bonding	L1	5.8053E-8	0.62323	144.27	23.865
	L2	5.8053E-8	0.62323	144.27	23.865
unbalanced cross bonding	L1	5.8126E-8	0.62323	144.27	23.865
	L2	5.8126E-8	0.62323	144.27	23.865

analyses and discusses the findings of a study on how sheath cross-bonding affects I_{ZS} in twin-circuit systems.

In case of balanced cross-bonding; Fig. 13a shows the result of the I_{ZS} flows at cables L1 and L2 in case (4) and Fig. 13b shows the result of the I_{ZS} flows at the sheath. Also, Fig. 14a shows the result of the I_{ZS} flows at cables L1 and L2 in case (8) and Fig. 14b shows the result of the I_{ZS} flows at the sheath.

In case of unbalanced crossbonding, Fig. 15a shows the result of the I_{ZS} flows at cables L1 and L2 in case (4) and Fig. 15b shows the result of the I_{ZS} flows at the sheath. Also, Fig. 16a shows the result of the I_{ZS} flows at cables L1 and L2 in case (8) and Fig. 16b shows the result of the I_{ZS} flows at the sheath.

The calculated results for I_{ZS} in twin-circuit systems for different cable configurations are shown in Table 12. The table shows that, assuming balanced cross bonding is used, the sheath current at the arrangement of case (8) of big I_{ZS} is approximately ten times greater than that by configuration of case (4) of no I_{ZS}. However, the I_{ZS} in the circuit of unbalanced cross-bonding is not affected by the cable arrangement. However, in the design of case (8) where the I_{ZS} is considerable, the sheath circulation current between circuits is practically constant, at roughly 24 A, and irrespective of the imbalance ratio. While no sheath current circulates in the configuration of case (4).

6. Conclusions

By using ATPDraw analysis, an I_{ZS} produced in cable networks is investigated. It is obvious from the estimated findings that cable networks' unusually big I_{ZS} generation is caused by an unbalanced mutual coupling of two circuits. In order to decrease the mutual coupling unbalance, which in turn reduces the I_{ZS}, cable layouts are studied. The best cable configuration is determined to be effective in reducing the I_{ZS}. The conclusions are as follows:

(1) In a twin-circuit system, a I_{ZS} circulates between two circuits of cables and is lowered to almost zero with a symmetrical phase configuration.
(2) In a four-circuit system, unlike a twin-circuit system, even with symmetrical phase arrangement, the I_{ZS} cannot be lowered to zero.
(3) The I_{ZS} is not significantly affected by any unbalanced crossbonding.

Authors contribution

Shimaa A. F. Salem: data curation, resources, writing- original draft preparation; *Rabab R. M. Eiada*: conceptualization, investigation; Ebrahim *A. Badran*: review and editing the manuscript. All authors have read and agreed to the published version of the manuscript.

Conflicts of interest

The author declared that there are no potential conflicts of interest with respect to the research authorship or publication of this article.

References

Badran, E.A., Abdel-rahman, M.H., Dec. 2010. A power quality detection method for grid-connected wind farms. International Journal of Power Engineering and Green Technology (IJPEGT) 1 (2), 65–72. International Sciences Press.

Bernadelli, R., Conroy, E., Lowe, D., Galloway, J., 1997. Control modernization of SCR rectifiers with continuous device current monitoring. In: Record of Conference Papers. IEEE Industry Applications Society 44th Annual Petroleum and Chemical Industry Conference, 15-17 September 1997, Banff, AB, Canada, pp. 183–190. https://doi.org/10.1109/pcicon.1997.648182. IEEE.

Cable, L.S., 2009. High Temperature & Low Sag Aluminum Alloy Conductor. Seoul, South Korea, pp. 7–13. http://www.brasilco.com.br/images/equipamentos-ls-.

Gouramanis, K.V., Kaloudas, C.G., Papadopoulos, T.A., Papagiannis, G.K., Stasinos, K., 2011. Sheath voltage calculations in long medium voltage power cables. In: 2011 IEEE PES Trondheim PowerTech Power Technol. a Sustain. Soc. POWERTECH 2011, pp. 1–7. https://doi.org/10.1109/PTC.2011.6019234.

Kaloudas, C.G., Papadopoulos, T.A., Gouramanis, K.V., Papagiannis, G.K., Stasinos, K., 2011. Simulation of switching and lightning transients in parallel single-core underground cables. In: Proceedings of the 46th International Universities' Power Engineering Conference (UPEC), 05-08 September 2011, VDE, Soest, Germany.

Ledari, S.A., Mirzaie, M., 2020. Sheath induced voltage prediction of high voltage cable based on artificial neural network. Comput. Electr. Eng. 87, 106788. https://doi.org/10.1016/j.compeleceng.2020.106788.

Li, Z., Zhong, X., Xia, J., Bian, R., Xu, S., Cao, J., 2015. Simulation of current distribution in parallel single-core cables based on finite element method. In: Proceedings - 2015 Fifth International Conference on Instrumentation and Measurement, Computer, Communication and Control (IMCCC), 18-20 September 2015, Qinhuangdao, China. IEEE, pp. 411–415. https://doi.org/10.1109/IMCCC.2015.94.

Nakanishi, H., et al., 1991. A study of zero-sequence current induced in a cable system. IEEE Trans. Power Deliv. 6, 1352–1358. https://doi.org/10.1109/61.97663.

Nexans, S.A., 2009. 6–36 kV Medium Voltage Underground Power Cables. https://www.powerandcables.com/wp-content/uploads/2016/12/Nexans-6-33kV-Medium-High-Voltage-Underground-Power-Cables.pdf. vol. 48.

Petty, K.A., 1988. Power Plant Electrical Reference Series. Palo Alto, CA Elect Power Res Inst. Volume 1–5.

Rifaldi, A., Lastra, R.B., 2001. Electronic Edition of the ATP Rulebook in PDF Forma. Rev. Iberoam del ATP File RB-01H.

Salem, S.A.R., Eiada, R.R., Badran, E.A.G., 2022. A proposed method for reduction of induced zero-sequence current in

cable system. Int. J. Power Electron. Drive Syst. 13, 2071−2078. https://doi.org/10.11591/ijpeds.v13.i4.pp2071-2078.

Shokry, M.A., Khamlichi, A., Garnacho, F., Malo, J.M., Alvarez, F., 2019. Detection and localization of defects in cable sheath of cross-bonding configuration by sheath currents. IEEE Trans. Power Deliv. 34, 1401−1411. https://doi.org/10.1109/TPWRD.2019.2903329.

Skibinski, G.L., Brown, B., Christini, M., 2006. Effect of Cable Geometry on Induced Zero Sequence Ground Currents with High Power Converters. IEEE. https://doi.org/10.1109/PCICON.2006.359703.

Tambe, S., Frisch, J., 2004. Upgrading rectifier systems - how to improve efficiency, increase reliability and reduce down time. In: Fifty-First Annual Conference 2004 Petroleum and Chemical Industry Technical Conference, 2004, San Francisco, CA, USA. IEEE, pp. 119−125. https://doi.org/10.1109/pcicon.2004.1352787.

Indian standard for hard-drawn copper conductors for overhead power transmission, 1982. https://www.slideshare.net/vasavachirag30/indian-standard-for-harddrawn-copper-conductors-for-over-head-power-transmission#.